



HAL
open science

Simulation of argon induced coupling coefficients of NH₃ doublets and their speed dependence

Franck Thibault, Alexandra Viel, Christian Boulet

► **To cite this version:**

Franck Thibault, Alexandra Viel, Christian Boulet. Simulation of argon induced coupling coefficients of NH₃ doublets and their speed dependence. *Journal of Quantitative Spectroscopy and Radiative Transfer*, 2023, 296, pp.108453-1-12. 10.1016/j.jqsrt.2022.108453 . hal-03880274

HAL Id: hal-03880274

<https://hal.science/hal-03880274>

Submitted on 5 Dec 2022



HAL is a multi-disciplinary open access archive for the deposit and dissemination of scientific research documents, whether they are published or not. The documents may come from teaching and research institutions in France or abroad, or from public or private research centers.

L'archive ouverte pluridisciplinaire **HAL**, est destinée au dépôt et à la diffusion de documents scientifiques de niveau recherche, publiés ou non, émanant des établissements d'enseignement et de recherche français ou étrangers, des laboratoires publics ou privés.



Distributed under a Creative Commons Attribution - NonCommercial - NoDerivatives 4.0 International License

Simulation of argon induced coupling coefficients of NH₃ doublets and their speed dependence

Franck Thibault ^a, Alexandra Viel ^a, Christian Boulet^b

^aUniv Rennes, CNRS, IPR (Institut de Physique de Rennes)-UMR 6251, F-35000 Rennes, France

^bInstitut des Sciences Moléculaires d'Orsay, CNRS, Université Paris-Saclay, F-91405 Orsay, France.

Abstract

We present a theoretical evaluation of collision induced effects on a few typical doublets in the ν_4 band of ammonia perturbed by argon. Quantum dynamical calculations performed on two NH₃-Ar potential energy surfaces provide pressure broadening and intradoublet generalized cross sections. From these calculations we derive thermally averaged values at various temperatures. The intradoublet coupling terms at room temperature are found to be in good agreement with available data in the literature. In addition, we study the speed dependence of the pressure broadening and intradoublet coupling coefficients. The former show a usual speed dependence, quite important, but the later show a weak speed dependence at least around 296 K and above.

doi: [10.1016/j.jqsrt.2022.108453](https://doi.org/10.1016/j.jqsrt.2022.108453)


Keywords: Ammonia, NH₃-Ar, Collisional Broadening, Line Mixing, Speed Dependence, Quantum Dynamical Calculations

1. Introduction

The last decades have seen a large number of studies devoted to the interaction of ammonia with argon. Several potential energy surfaces were produced, that allow the calculations of differential and integral cross sections, of the heterodimer spectra, and the comparison with experimental data, (for a review see [1–3]). The perturbation of the monomer spectra of NH₃ surrounding by argon led to numerous studies (for a review see [4, 5]), most of them being devoted to the collisional broadening and shift of rovibrational lines. A few studies were also devoted to the overall band perturbation due to line mixing [6–9]. Since the pioneering works of Baranger [10, 11] on overlapping lines and in particular of Ben Reuven [12] on ammonia inversion doublets, a special attention has been paid to couplings between such lines. Following the latter, quite recently a renewed interest of line mixing in symmetric top spectra has been the subject of theoretical works based on semi-classical methods [13–18]. If the speed dependence of the line broadening and shift coefficients is nowadays commonly included in various line shape models [4, 5], the speed dependence of off-diagonal relaxation matrix elements that lead to line couplings is disregarded [19]. In 2021, Boulet et al [20] have suggested that this effect could be detected in some doublets of the ν_4 band of ammonia in argon. However in the absence of any theoretical prediction, that study was based on the assumption that the speed dependence of the coupling between the two components of a doublet was identical to that of the width and could be modeled by hypergeometric or quadratic laws.

In the present paper, performing quantum dynamical calculations on two different potential energy surfaces (PESs) [1, 21] we determine some generalized spectroscopic cross sections and more particularly the 2x2 W relaxation matrix elements for some $^P P(j, k)$ doublets of the ν_4 band. We believe that this is the first ab initio tentative simulation of intradoublet line couplings as well as of their speed dependence. The magnitude of the reported intradoublet relaxation matrix elements are in overall good agreement with previously determined ones either experimentally or semi-empirically [6, 9] at room temperature. While the speed dependence of the pressure broadening coefficients is well pronounced and can be indeed represented by either the hypergeometrical function derived from classical or semi-classical methods [22–24] or the ad hoc [25] quadratic function adopted by the HITRAN database [26] this is not at all the case for the off-diagonal (intradoublet) relaxation matrix elements. Moreover, the speed dependence of the later is found to be small precluding their experimental determination at least at room temperature.

Section 2 of this paper describes the followed methodology. We first briefly describe and compare the PESs used. Then we remind the reader the rotational energy level structure and the rotation-inversion basis. Expressions of the generalized spectroscopic cross sections are given in Sec. 2.3 followed by a short summary of the actual calculations we have performed. Section 3 presents our results, including some typical examples of kinetic energy dependent cross sections, their speed dependence and the thermally averaged values. Finally, section 4 provides a short conclusion.

Email address: franck.thibault@univ-rennes1.fr (Franck Thibault )

2. Methodology

In the following subsections the evaluation of line broadening and mixing parameters of a selection of ammonia doublets is detailed. Table **T1** in the Supplementary Material provides the position and quantum numbers associated to the 14 studied lines. In addition to the usual rotational quantum number j , k the absolute value of its projection K on the symmetry axis, and the symmetry index ϵ , a label s/a , standing for symmetric and antisymmetric, is necessary to specify the symmetry with respect to the inversion motion of NH_3 . The relevant ν_4 vibrational mode is a doubly degenerate bending mode. And the so-called ν_4 band is a perpendicular band due to infrared active dipole electric transitions for which the radiative selection rules $s \rightarrow s$ and $a \rightarrow a$, $\Delta j = 0, \pm 1$ and $\Delta K = \pm 1$ apply. In addition, in the final vibrational level, the vibrational angular momentum is excited $l_4 = \pm 1$. Moreover, this band is strongly affected by perturbations due to the vicinity of the ν_2 (s) band [27]. Of course, our study disregards the possible related effects on the considered lines.

2.1. Potential energy surfaces used

Following our previous work [7], most of our dynamical calculations were performed on the potential energy surface (PES) determined by Schmuttenmaer et al. [21]. In addition, we repeated a few of them using the more recent PES of Loreau et al. [1]. The former PES is derived from fitting observed transitions of the van der Waals complex with ammonia in its ground vibrational state and second virial coefficients whereas the later is a pure *ab initio* prediction. The analytical fit chosen in the semi-empirical PES based on Jacobi coordinates makes it suitable for direct implementation in Molscat codes [28, 29]. Indeed, this potential uses the 3 Jacobi coordinates R, θ, ϕ to localise the Ar atom with respect to the NH_3 molecule. Namely, \vec{R} joins the center of mass of ammonia to the argon atom and defines the z-collisional axis, θ is the angle formed by \vec{R} and the C_3 symmetry axis, and finally ϕ describes the rotation of the Ar atom around the later axis. The 3-dimensional PES of Schmuttenmaer et al. [21] does not depend explicitly on the coordinate describing the inversion-tunneling motion (see figure 1 of Ref. [21]). The surface of Loreau et al. [1] contains the explicit dependence upon the umbrella inversion ρ . The fitting expansion relies on a second set of Jacobi coordinates, defined with respect to the N atom but a simple geometrical coordinate transformation is done [1] in order to recover the coordinates suitable for scattering calculations. In our calculation the umbrella angle was set to its averaged value in the vibrational ground state, $\rho = 111.4^\circ$. Note that the N-H bond length is also fixed to its average value, $r_0 = 1.9204 a_0$. Figure **F1** in the Supplementary Material compares selected angular cuts of the two PESs used. One can check that they differ only slightly.

Because we are using 3-dimensional PESs, but wish to include the inversion motion we apply the model developed by Davis and Boggs [30] for this purpose. Therefore, the inversion motion is approximated by the delta function model [30] that expresses the inversion wave functions as linear combinations

of the equilibrium structure (see detailed discussions in references [2, 21, 31–33]).

For our dynamical calculations the 3-dimensional PESs have been expanded over spherical harmonics:

$$V(R, \theta, \phi) = \sum_{\lambda, \mu \geq 0} v_{\lambda\mu}(R) (1 + \delta_{\mu,0})^{-1} [Y_{\lambda\mu}(\theta, \phi) + Y_{\lambda, -\mu}(\theta, \phi)], \quad (1)$$

where due to the C_{3v} symmetry $\mu = 3n$ (n integer). The expansion has been carried out up to $\lambda = 7$, leading to a maximum of 15 radial potential coefficients. The collisional selection rules induced by such a potential cannot interconvert ortho- and para- NH_3 . This is a very interesting feature because it allows separate dynamical calculations (Molscat runs) for the 2 species, reducing the computational cost. Figure 1 shows their main radial coefficients¹ as defined in Eq. (1). Overall, these coefficients are very similar. Slight divergence is observed at very short range for instance for the V_{33} anisotropic components, but these components, at such distances, are screened by their respective isotropic component.

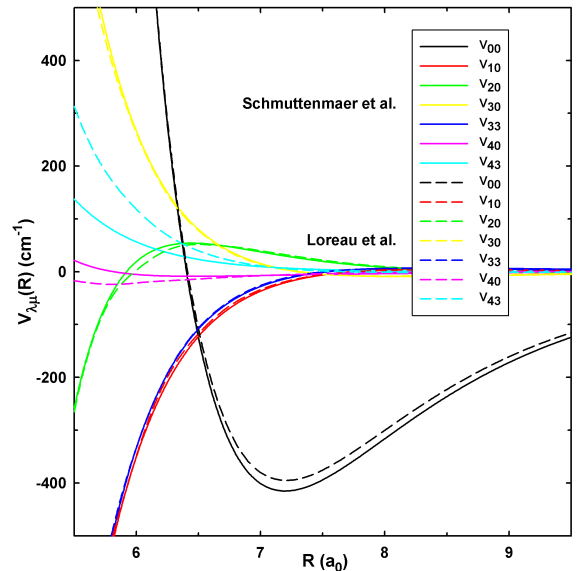


Figure 1: Comparison of the most important radial coefficients (Eq. (1)) for the PESs of Schmuttenmaer et al. [21] and Loreau et al. [1].

The quality of the Schmuttenmaer et al. [21] and of the Loreau et al. [1] surfaces has been demonstrated in previous works. The semi-empirical surface of Schmuttenmaer et al. [21] is build using experimental data and has been shown to properly reproduce differential and integral cross sections that compare well with experimental values as clearly demonstrated in Ref. [34]. Similarly the quality of the *ab initio* surface of Loreau et al. has been demonstrated using spectroscopic energy levels of NH_3 and ND_3 -Ar complexes [1], rotationally inelastic scattering measurements [35] and spectroscopic constants of the heterodimer in the region of the ν_2 monomer's band [3].

¹All the energies are expressed in units of E/hc , where c is the speed of light in cm.

2.3. Generalized spectroscopic cross sections

First, for future discussion we remind the reader the standard inelastic cross section expression in the close coupling (CC) scheme, $\vec{J} = \vec{j} + \vec{\ell}$, for a collisional transition from a state i to a state i' is given by:

$$\sigma(i' \leftarrow i; E_{kin}) = \frac{\pi}{g_i \kappa_i^2} \sum_J \sum_{\ell, \ell'} (2J+1) |S^J(i' \ell', i \ell)|^2, \quad (3)$$

where g_i is the degeneracy factor of the initial level, κ_i is the modulus of the wave vector associated with the initial kinetic

energy $E_{kin} = (\hbar \kappa_i)^2 / 2\mu_r$, with $\mu_r = 11.9396$ u, the reduced mass of the $\text{NH}_3\text{-Ar}$ system, and ℓ designates a relative angular momentum.

Within the impact approximation (for a review see Refs. [4, 40]) the generalized cross section coupling a line $|l\rangle \equiv |j_i k_i m_i \epsilon_i, j_f k_f m_f \epsilon_f\rangle$ for a given radiative transition from a state i to a state f with a line $|l'\rangle \equiv |j_{i'} k_{i'} m_{i'} \epsilon_{i'}, j_{f'} k_{f'} m_{f'} \epsilon_{f'}\rangle$ for a transition from i' to f' in the case of a symmetric top interacting with a structureless atom is given by:

$$\begin{aligned} \sigma^{(q)}(l', l; E_{kin}) = & \frac{\pi}{\kappa_i^2} \left(\frac{[j_{i'}]}{[j_i]} \right)^{\frac{1}{2}} \times \sum_{J_i J_f \ell \ell'} [J_i] [J_f] (-1)^{j_i - j_{i'} + \ell - \ell'} \left\{ \begin{matrix} j_{i'} & q & j_{f'} \\ J_f & \ell' & J_i \end{matrix} \right\} \left\{ \begin{matrix} j_i & q & j_f \\ J_f & \ell & J_i \end{matrix} \right\} \\ & \times \left[\delta_{i'i'} \delta_{f'f} \delta_{\ell \ell'} - \langle j_{i'} k_{i'} \epsilon_{i'} \ell' | S^{J_i}(E_{T_i}) | j_i k_i \epsilon_i \ell \rangle \langle j_{f'} k_{f'} \epsilon_{f'} \ell' | S^{J_f}(E_{T_f}) | j_f k_f \epsilon_f \ell \rangle^* \right]. \quad (4) \end{aligned}$$

In Eq. (4) $[X]$ stands for $2X+1$, $\{ : : \}$ refers to 6-j symbols. q designates the order of the radiative-matter interaction and equals 1 in the present study of electric dipole transitions. The total energy in the initial channel i is $E_{T_i} = E_{kin} + E_{rot_i}$ while $E_{T_f} = E_{kin} + E_{rot_f}$ is the total energy in the final channel f . Scattering matrix elements are thus evaluated at these energies. Primes denote post-collision states. The end-over-end relative kinetic angular momentum are denoted ℓ and ℓ' . Paraphrasing Green [36], Eq. (4) is similar to the well known expression for a diatom-atom system, with the additional k, ϵ labels in the brackets, because " k acts as a spectator in the angular coupling". The coupled states (CS) expression of such a cross section for a symmetric top perturbed by an atom is thus not repeated here, it can be deduced from equation (10) of Ref. [37] by merely adding ϵ .

In the rest of this article we will only discuss the real part of the cross sections and thus of the relaxation matrix elements (RMEs). Indeed, for instance, the line shifts are very sensitive to the vibrational dephasing [4] but the PESs used have no vibrational dependence.

As it is well known, (the real part of) a diagonal, i.e. setting $|l\rangle = |l'\rangle$ in Eq. (4), generalized cross section yields the pressure broadening (PB) cross section. The PB cross section, is the sum of two contributions, a first one coming from inelastic collisions and a dephasing contribution coming from elastic collisions [10–12, 41, 42]:

$$\sigma^{(q)}(l, l; E_{kin}) = \sigma_{inel} + \sigma_{deph}^{(q)}, \quad (5)$$

with

$$\sigma_{inel} = \frac{1}{2} \left(\sum_{i' \neq i} \sigma(i' \leftarrow i) + \sum_{f' \neq f} \sigma(f' \leftarrow f) \right). \quad (6)$$

There is no such decomposition for off-diagonal cross sections. However, for isotropic Raman Q lines, $q = 0, i = f, i' = f', i \neq i'$, neglecting any vibrational effect, one can easily show that:

$$\sigma^{(0)}(l', l; E_{kin}) = -\sigma(i' \leftarrow i; E_{kin}) \quad (7)$$

For electric dipole transitions, $q = 1$, such a simple relation does not exist but physically the coupling between 2 lines clearly comes from inelastic collisions and S -matrix elements that enter into Eq. (4) are the same that lead to the state to state cross sections $\sigma(i' \leftarrow i)$ and $\sigma(f' \leftarrow f)$ (Eq. (3)).

Finally, for future use, we define for two lines $|l\rangle$ and $|l'\rangle$ constituting a doublet the intradoublet inelastic (IDI) contribution to the inelastic part of the diagonal cross section (Eq. (6)):

$$\sigma^{IDI}(l', l; E_{kin}) = \frac{1}{2} (\sigma(i' \leftarrow i; E_{kin}) + \sigma(f' \leftarrow f; E_{kin})). \quad (8)$$

The negative of this expression can also be compared to Eq. (7).

2.4. Dynamical calculations performed

The necessary cross sections were calculated with the Molscat codes [28, 29] for kinetic energies in the range 0-1800 cm^{-1} . The kinetic energies have been sampled on a non regular grid. For energy below 20 cm^{-1} , we evaluated the cross sections every 0.5 cm^{-1} while steps of 250 cm^{-1} have been used for energies above 1000 cm^{-1} . Special attention was paid near the thresholds. The coupled state (CS) approximation was used for kinetic energies greater than ~ 800 cm^{-1} . Additional CS calculations were also performed at smaller ones to check the accuracy of this approximation (see below). The S^J -matrix blocks are considered as converged when the contributions to the diagonal and off-diagonal state to state cross sections are smaller than 0.1 and 0.01 \AA^2 respectively. We used the hybrid log-derivative/Airy propagator [43, 44] starting at $R = 2.5$, switching at 40 and ending at 100 \AA . The propagator step size was adapted with the kinetic energy: we used more than 25 points per half wavelength below 10 cm^{-1} and 10 points above 1000 cm^{-1} . At least 10 energetically closed levels were included in our basis⁴.

⁴For instance at a total energy of 600 cm^{-1} a Molscat CC run lasts 7.5h, including 62 levels, and converges at $J = 169$.

3. Results

Table 1: Lines for which cross sections were calculated.

Initial lines	Final lines
${}^P P(3, 3)_s$	${}^P P(3, 3)_{s,a}$
${}^P P(4, 2)_{s,a}$	${}^P P(4, 2)_{s,a}$
	${}^P P(5, 5)_{s,a}$
${}^P P(5, 2)_{s,a}$	${}^P P(5, 2)_{s,a}$
	${}^P P(5, 5)_{s,a}$
${}^P P(5, 5)_{s,a}$	${}^P P(4, 2)_{s,a}$
	${}^P P(5, 2)_{s,a}$
	${}^P P(5, 5)_{s,a}$
${}^P P(6, 5)_s$	${}^P P(6, 5)_{s,a}$
${}^P P(6, 6)_s$	${}^P P(6, 6)_{s,a}$
${}^P P(8, 8)_s$	${}^P P(8, 8)_{s,a}$

3.1. Kinetic energy dependent cross sections

The 36 cross sections for which calculations were performed are gathered in Table 1. We focus here on the intradoublet couplings and for some doublets the couplings with the nearest ones. As an illustrative example we consider the case of the ${}^P P(5, 5)_s$ line.

Cross sections involving the ${}^P P(5, 5)_s$ line are plotted on Fig. 2 and 3. First, we observe that the CS approximation works well (in fact, we have checked that the CS state to state cross sections are already in quite good agreement with the CC ones above 300 cm^{-1}). Generally speaking, the CSA is expected to be accurate when the kinetic energy is large compared to the well depth, $\sim 110 \text{ cm}^{-1}$ for the isotropic part of the present system. This is not surprising in view of previous studies on $\text{NH}_3\text{-He}$ state to state or pressure broadening cross sections [36, 37, 45] and for the $\text{NH}_3\text{-Ar}$ system [32].

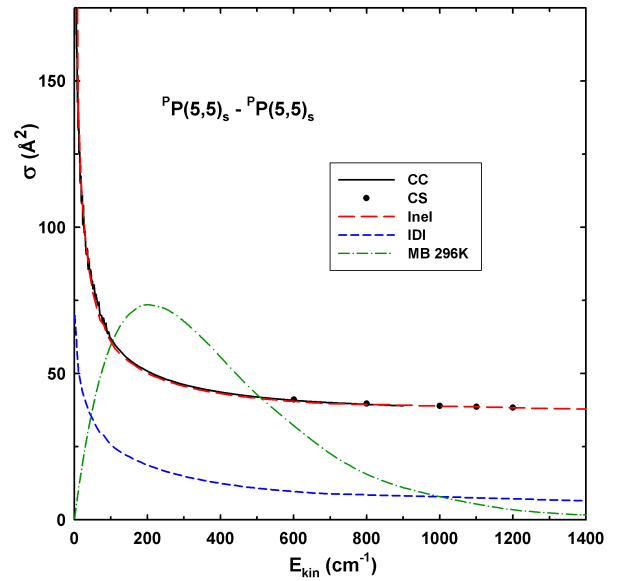


Figure 2: Cross sections for the ${}^P P(5, 5)_s$ line obtained with the Schmuttenmaer *et al.* [21] PES as a function of the kinetic energy. Real part of the diagonal cross section is evaluated with the CC method (black solid line) and with the CSA (black solid disks). The total inelastic contribution (Inel, Eq. (6)) is presented in red dashed line and the contribution from the intradoublet inelastic (IDI) cross section in blue dashed line. The relevant Maxwell-Boltzmann (MB) kinetic energy distribution at 296 K is displayed by the green dash-dotted line.

Focusing on Fig. 2 which provides the real part of the diagonal cross section as a function of the kinetic energy for the ${}^P P(5,5)_s$ line, we note that the neglect of the dephasing contribution works well for this system even at quite low kinetic energies and thus the inelastic contributions to the PB cross sections are largely dominant. This is due to the 2 large intradoublet inelastic cross sections $\sigma(55-1 \leftarrow 551)$ and $\sigma(441 \leftarrow 44-1)$ and to the numerous downward inelastic cross sections. Green [31] already noticed that considering only the inelastic contribution given by Eq. (6) is accurate for ammonia in helium baths at room temperature. As also pointed out in the later reference, the pressure broadening of a line does not reduce to the half sum of the inelastic cross sections between the levels of the considered doublet, Eq. (8) (dashed blue line on Fig. 2). In fact, in the case of NH_3 perturbed by He this part of the total inelastic contribution accounts to about 50% of the inelastic contribution to the PB cross section. Present detailed calculations for NH_3 in Ar prove that intradoublet inelastic cross sections account to $\sim 45\%$ of the total inelastic contribution to the PB cross section at a kinetic energy of 50 cm^{-1} and this percentage falls down

to $\sim 25\%$ at 500 cm^{-1} , compare the blue (IDI) and red dashed (Inel) lines on Fig. 2. This variation with the kinetic energy is confirmed by the blue curve on Fig. 4 which represents the ratio of the intradoublet inelastic cross section to the pressure broadening one.

We now consider off-diagonal cross sections involving the ${}^P P(5,5)_s$ line, see left panel of Fig. 3. The intradoublet coupling is much bigger than the coupling with other lines. This can be attributed to a much closer spacing of the energy levels involved in the doublet transitions, of the order of 0.8 cm^{-1} and strong coupling due to the ν_{10} and ν_{30} radial terms. Consequently, at not too high pressure, at least below 1 atmosphere, one may just consider the intradoublet coupling and disregard the line mixing with other lines. The ${}^P P(5,5)_s$ line can be coupled with the ${}^P P(5,2)_{s/a}$ lines if the kinetic energy is larger than 78 cm^{-1} corresponding to the energy difference between the $55+1$ and $52+1$ levels (see the Supplementary Material, Fig. F2). This threshold is clearly visible on the left panel of Fig. 3 for the two relevant cross sections.

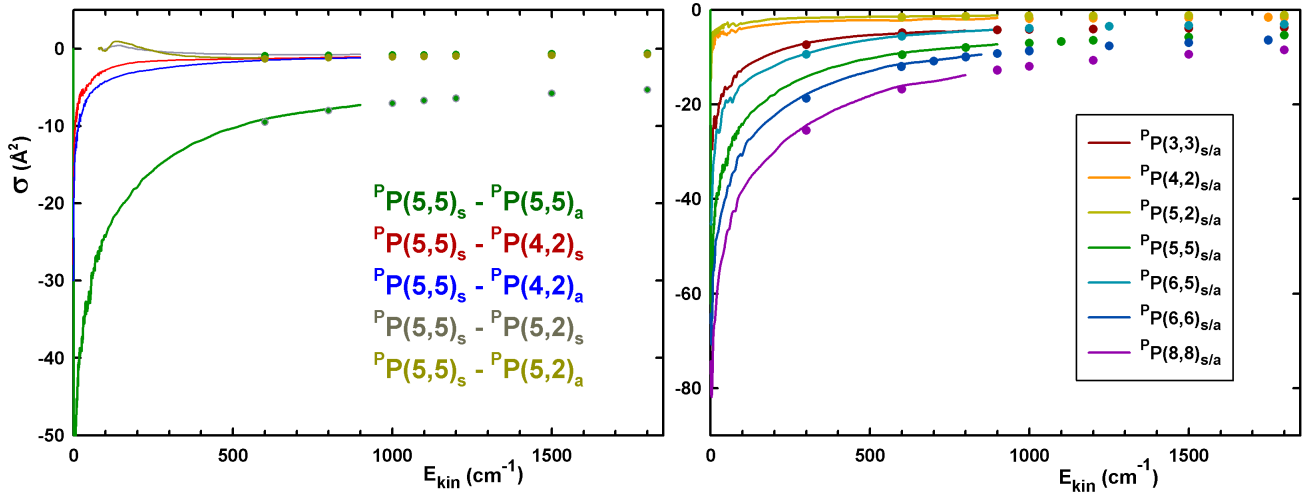


Figure 3: Kinetic energy dependent off-diagonal cross sections obtained with Schmuttenmaer et al. [21] PES. Left panel: coupling cross sections of the ${}^P P(5,5)_s$ with other studied lines. Right panel: intradoublet cross sections. Solid lines: CC values, solid disks: CSA values.

The cross sections involving the ${}^P P(5,5)_a$ initial line, not shown, are similar to the ones plotted on Fig. 2 and 3. The coupling of the ${}^P P(5,5)_a$ line to the ${}^P P(5,5)_s$ line is very close to the one for the reverse coupling. For the other couplings, the s/a label has to be exchanged, namely, ${}^P P(5,5)_s - {}^P P(4,2)_s$ is similar to ${}^P P(5,5)_a - {}^P P(4,2)_a$, and so on. An off-diagonal generalized cross section (Eq. (4)) is not a standard inelastic cross section (Eq. (3)) but the former cross section clearly comes from off-diagonal S-matrix elements that also enter in the 2 related inelastic cross sections. Therefore, the last observation must be related to the fact that symmetry considerations impose that in absence of s/a energy splittings, the state to state cross section $\sigma(j'k'e' \leftarrow jk\epsilon)$ is equal to $\sigma(j'k' - \epsilon' \leftarrow jk - \epsilon)$

[36]. This strict rule is waived as soon as the splitting due to the vibration-inversion motion is taken into account. In case of small splittings like in the present NH_3 case, our calculations confirm that the above equality is still valid within a few percents. This point was already discussed in ref. [32].

We extend the link between standard cross sections and off-diagonal spectroscopic cross sections with the following comparison: Fig. 4 provides the ratio of the off-diagonal cross section $\sigma^{(1)}({}^P P(5,5)_a, {}^P P(5,5)_s)$ to the diagonal one $\sigma^{(1)}({}^P P(5,5)_s, {}^P P(5,5)_s)$ and the ratio of the intradoublet inelastic contribution $\sigma^{IDI}({}^P P(5,5)_a, {}^P P(5,5)_s)$ to the same pressure broadening cross sections. What is striking on Fig. 4 is that the 2 ratios are very close. In other words, the IDI contribu-

tion nearly equals the intradoublet cross section. Note that this is the way the intradoublet relaxation matrix element were approximated in [6], with the addition of a scaling factor. Such an ad hoc procedure has been adopted in many previous works [4, 46]. This approximation is more accurate as the kinetic energy increases (see Fig. 4), fact that we have also verified for other doublets.

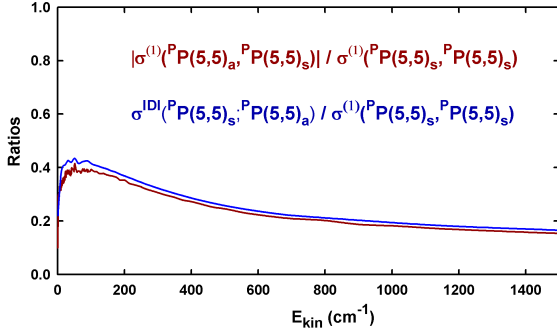


Figure 4: Ratios, as a function of the kinetic energy, of the coupling cross section of the ${}^P P(5,5)_s$ with its companion line, ${}^P P(5,5)_a$ to the PB cross section of the former and of the intradoublet inelastic contribution, Eq. (8), to the PB cross section.

The right panel of Fig. 3 provides the off diagonal cross sections of the intradoublet studied. It clearly appears that these cross sections have the same variation with the kinetic energy. The strength of the intradoublet cross sections do not depend only on the spacing between the 2 lines. Following Lightman et al. [47] for a given j value, the intradoublet coupling coefficient should increase with k , what we observe. More recently, Ma et al. [16, 18] have shown that the intradoublet couplings increase with j and k . The intradoublet state to state cross sections are mostly governed by the direct processes due to the $\nu_{10}Y_{10}$ and $\nu_{30}Y_{30}$ potential coupling terms (see Eq. 26 of [36] and [30, 31, 38]). On this basis the coupling should increase with j and k .

Finally, we have checked the influence of the potential energy surface by repeating the determination of the cross sections involving the ${}^P P(5,5)_{s/a}$ lines and the cross sections for the ${}^P P(3,3)_{s/a}$ doublet with the *ab initio* PES of Loreau et al. [1]. The obtained results are very similar. We thus conclude that for the current purposes the semi-empirical potential is as accurate as the *ab initio* one.

3.2. Relaxation matrix

A first step towards a comparison with experimental data, in particular the PB coefficients, is to provide thermally averaged values. To this end we calculate the relaxation matrix elements [4, 12, 40, 48]:

$$\langle\langle l' | W^{(1)} | l \rangle\rangle = \frac{n\bar{v}_r}{2\pi c} \langle \sigma^{(1)}(l', l; E_{kin}) \rangle \quad (9)$$

where n is the argon density number and \bar{v}_r the mean relative speed at the temperature T which is given by $\sqrt{\frac{8k_B T}{\pi\mu_r}}$. The thermal average is performed over the Maxwell-Boltzmann kinetic

Table 2: Comparison of present calculated HWHM (half widths at half maximum) and available data. Values are given in $10^{-3} \text{ cm}^{-1} \text{ atm}^{-1}$. All the computations are performed using the Schmuttenmaer et al. PES [21] and the repeated ${}^P P(3,3)_s$ and ${}^P P(5,5)_s$ entries at the bottom of the table correspond to a computation with the Loreau et al. [1] PES.

Line	Present		Calc [15]	Exp [49]	Exp [6]
	193 K	296 K	296 K	296 K	296 K
${}^P P(3,3)_s$	71.15	50.49	55.7	55.2	55.3
${}^P P(4,2)_s$	64.76	47.06			
${}^P P(4,2)_a$		47.08	51.5	50.3	
${}^P P(5,2)_s$	59.10	43.62		46.4	
${}^P P(5,2)_a$		43.60	46.7	48.8	
${}^P P(5,5)_s$	63.43	46.23		53.6	48.0
${}^P P(5,5)_a$		46.24	49.5	54.4	
${}^P P(6,5)_s$	56.56	42.15	48.8	47.9	47.9
${}^P P(6,6)_s$	59.77	43.91	46.6	53.6	50.8
${}^P P(8,8)_s$	54.84	40.48	42.3	45.9	44.6
${}^P P(3,3)_s$	67.20	48.01	55.7	55.2	55.3
${}^P P(5,5)_s$	60.69	44.18		53.6	48.0

energies distribution,

$$\langle \sigma^{(1)}(l', l; E_{kin}) \rangle = \frac{1}{(k_B T)^2} \int_0^\infty E_{kin} e^{-E_{kin}/k_B T} \sigma^{(1)}(l', l; E_{kin}) dE_{kin}. \quad (10)$$

Given the kinetic energies grid used, relaxation matrix elements at any temperature in the range 10 - 350 K are expected to be converged, and with an improved accuracy in the range 50 to 300 K.

Before going further we compare in Table 2 the diagonal relaxation matrix elements with collisional broadening coefficients, measured at room temperature, available in the literature. As expected the results do not present any significant s/a dependence for the doublets. The present calculated values are clearly underestimating the HWHM because we restrict NH_3 to be rigid. The vibrational phase shift is thus missing. In addition to comparison with experimental values, Table 2 provides published theoretical results performed by Starikov [15] using semi-classical calculations. They are based on an empirical PES [49] for which the effective parameters were adjusted to provide reliable HWHM. For further studies we also provide in Table 2 our theoretical HWHM at 193 K obtained with the semi-empirical PES [21]. In addition, we provide the values, at 193 and 296 K, obtained with the *ab initio* PES of Loreau et al. [1] for the ${}^P P(3,3)$ and ${}^P P(5,5)$ doublets. We note that these PESs lead to close results. Similar to the other tests performed, the differences observed are not relevant for the HWHM and the semi-empirical PES is of sufficient quality.

We now briefly discuss off-diagonal relaxation matrix elements for the ${}^P P(5,5)_{s,a}$ initial lines with the other lines considered in this study. Conclusions are directly transposable to the other doublets. For all tested temperatures, we obtained $W({}^P P(5,5)_s, {}^P P(j,k)_{s,a}) \cong W({}^P P(5,5)_a, {}^P P(j,k)_{a,s})$. This results is not surprising given the comparisons of the involved cross sections as detailed in Sec. 3.1. In addition, the detailed

3.4.1. Dependence on the relative speed

Let us define a relative speed dependent relaxation matrix element w as:

$$w_{i,j}(v_r) = \frac{n}{2\pi c} v_r \sigma_{ij}(v_r), \quad (13)$$

with $i = 1, 2$ and $j = 1, 2$ and where v_r is the relative speed associated with the center of mass kinetic energy $E_{kin} = \frac{1}{2}\mu_r v_r^2$, and n is the density number of the perturbing atoms (Ar). In order to study the dependence on v_r , according to Eq. (13), we have plotted $\sqrt{E_{kin}}\sigma_{ij}$ vs $\sqrt{E_{kin}}$ on figure 5.

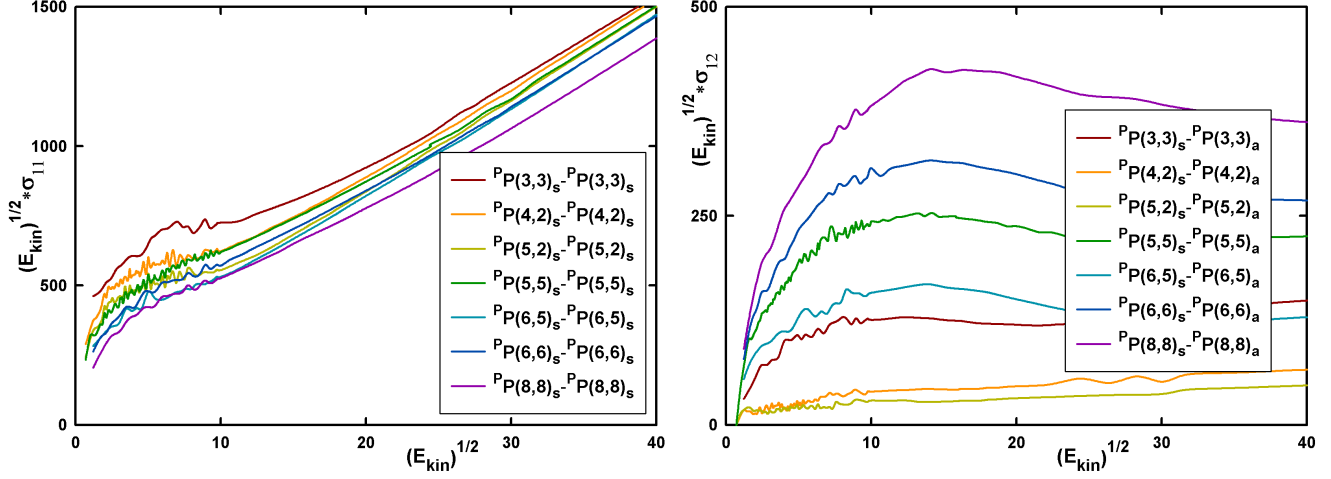


Figure 5: Relative speed dependence of diagonal, w_{11} (left panel), and off-diagonal, w_{12} (right panel), RMEs for the studied doublets. Results obtained with Schmuttenmaer et al. [21] PES.

As it appears immediately, the speed dependence of the diagonal and off-diagonal terms are totally different, as obviously could be already deduced examining Fig. 4, invalidating the assumption made in [20]. Schematically, we can distinguish two regimes. For small kinetic energies the w -matrix elements increase rapidly, then we observe an intermediate region strongly correlated with the opening above their threshold of the most efficient upward transitions. For higher kinetic energies the coupling elements exhibit a rather flat behavior ($w_{12}(v_r) \approx \text{constant}$), while the diagonal elements increase faster than linearly with the relative speed (approximately as $\sqrt{E}^{1.3}$).

As shown above (Fig. 2), disregarding the dephasing contribution, Eq. (5), the diagonal cross-section $\sigma_{11}(v_r)$ may be expressed as half the sum of the inelastic cross-sections starting from both the initial and final levels of the considered transition, which can be classified in two categories: downward and upward contributions. We expand below the inelastic contributions to the pressure broadening cross section (Eq. (6)):

$$\begin{aligned} \sigma_{11}(v_r) &= \frac{1}{2} \left\{ \sigma'_{out\ i}(v_r) + \sigma'_{out\ f}(v_r) \right\} \\ &= \frac{1}{2} \left\{ \sigma'_{out\ i}(v_r) + \sigma'_{out\ f}(v_r) \right\} + \sigma^{IDI}(v_r) \\ &= \frac{1}{2} \left\{ \sigma'_{down}(v_r) + \sigma'_{upw}(v_r) \right\} + \sigma^{IDI}(v_r) \end{aligned} \quad (14)$$

where the indices i and f are the initial and final states of the line $|1\rangle$, the indices 'out i ' ('out f ') designates the total inelastic cross section out of the state i (f), the intradoublet cross

section (IDI) has been defined in Eq. (8), and the index 'down' and 'upw' are the downward and upward cross sections out of i or f . Figure 6 shows this decomposition for the $^P P(5,5)_s$ line.

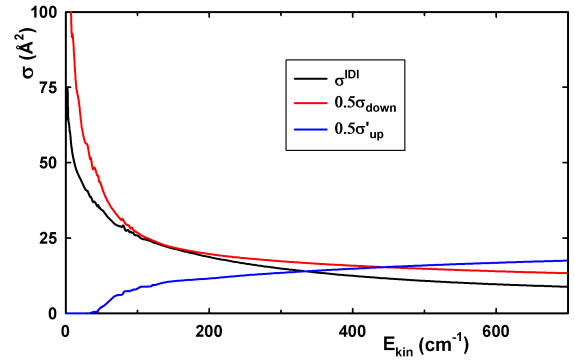


Figure 6: Illustration of Eq. (14) in the case of the $^P P(5,5)_s$ line. More detailed contributions are given in Fig. F4 of the Supplementary Material.

As can be seen, the half-sum of the downward inelastic cross sections out of the levels i and f (in red) and the intradoublet cross sections (in black) behave quite similarly with the kinetic energy. On the opposite the half-sum of the upward cross sections (in blue) strongly increases after their thresholds and then grows up slowly. Note that the next upper level may be not the one for which the state to state cross section is the largest because of the collisional selection rules and potential coupling

3.4.2. Dependence on the speed of the active molecule

Transforming a cross section which depends on the relative speed v_r , to a relaxation matrix element which depends on the absolute speed of the active molecule v , is done with the help of the function $f(v_r|v; T)$ [50] which provides the conditional probability that the relative speed is v_r when the active molecule speed is v at thermal equilibrium T :

$$w_{ij}(v; T) = \frac{n}{2\pi c} \int dv_r f(v_r|v; T) [v_r \sigma_{ij}(v_r)]. \quad (17)$$

Of course, from the latter relationship one can retrieve a thermally averaged relaxation matrix element :

$$W_{ij}(T) = \int dv F(v; T) [w_{ij}(v; T)], \quad (18)$$

where F is the Maxwell-Boltzmann distribution, at T , of the active molecule speed. When correctly handled Eq. (18) should provide the same results as Eq. (10).

Assuming a kinetic energy dependence of the cross sections as given by Eq. (??), the relative speed dependent relaxation matrix elements (Eq. (13)) vary as v_r^α , with $\alpha = 2a + 1$. Making use of Eq.(17) one obtains the active molecule speed dependence of w [22–24] at a given temperature:

$$w_{ij}(u, T) = W_{ij}(T) * (1 + \Lambda)^{-p} * M(-p; 3/2; -\Lambda u^2), \quad (19)$$

where $u = v/\tilde{v}$ is the reduced speed of the active molecule, with \tilde{v} its most probable speed at T ; Λ is the ratio of the perturber

mass to the active molecule mass; the first argument, p , of the confluent hypergeometric function M is related to the exponent α via $p = \frac{\alpha}{2}$. Finally, the overall factor $W_{ij}(T)$ is the thermally averaged relaxation matrix element (Eq.(18)).

As is well known, most of the studies devoted to speed dependent line shape are based on phenomenological models like that of Berman [22] for the speed dependence of the broadening. This model assumes resonant collisions and a radiator-perturber isotropic interaction potential dominated by a term proportional to R^{-N} driving straight line path trajectories. This models leads to the speed dependence given by Eq. (19) with [22–24]:

$$p = \frac{N - 3}{2N - 2}. \quad (20)$$

Thus one may relate (but must be cautious [24]) the above reasonable mathematical speed dependence with this phenomenological model. We also note that $N = 1 - \frac{1}{a}$ and that Eq. (19) is valid for $N > 1.5$. We remind the reader that for $a = -0.5$ (or a dipole-dipole interaction, $N = 3$) there is no speed dependence.

The present calculations give us the opportunity to test that hypergeometric model. We have therefore considered p and W_{11} as adjustable parameters which have been determined through a fitting procedure. Figure 8 gives the diagonal element $w_{11}(v; 296K)$ for the ${}^P P(5, 5)_s$ or a doublet as given by the present calculation and the result of the hypergeometric model.

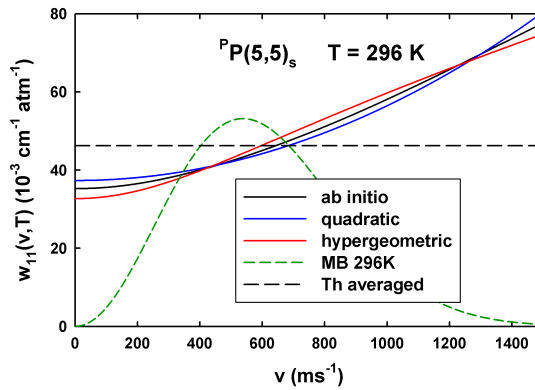


Figure 8: Speed dependence, at 296 K, of the pressure broadening coefficient of the ${}^P P(5, 5)_s$: *ab initio* results (black line), quadratic model (blue line), hypergeometric model (red line). In addition, the theoretical thermally averaged value is represented by the black dashed line and the speed distribution by the green dashed line.

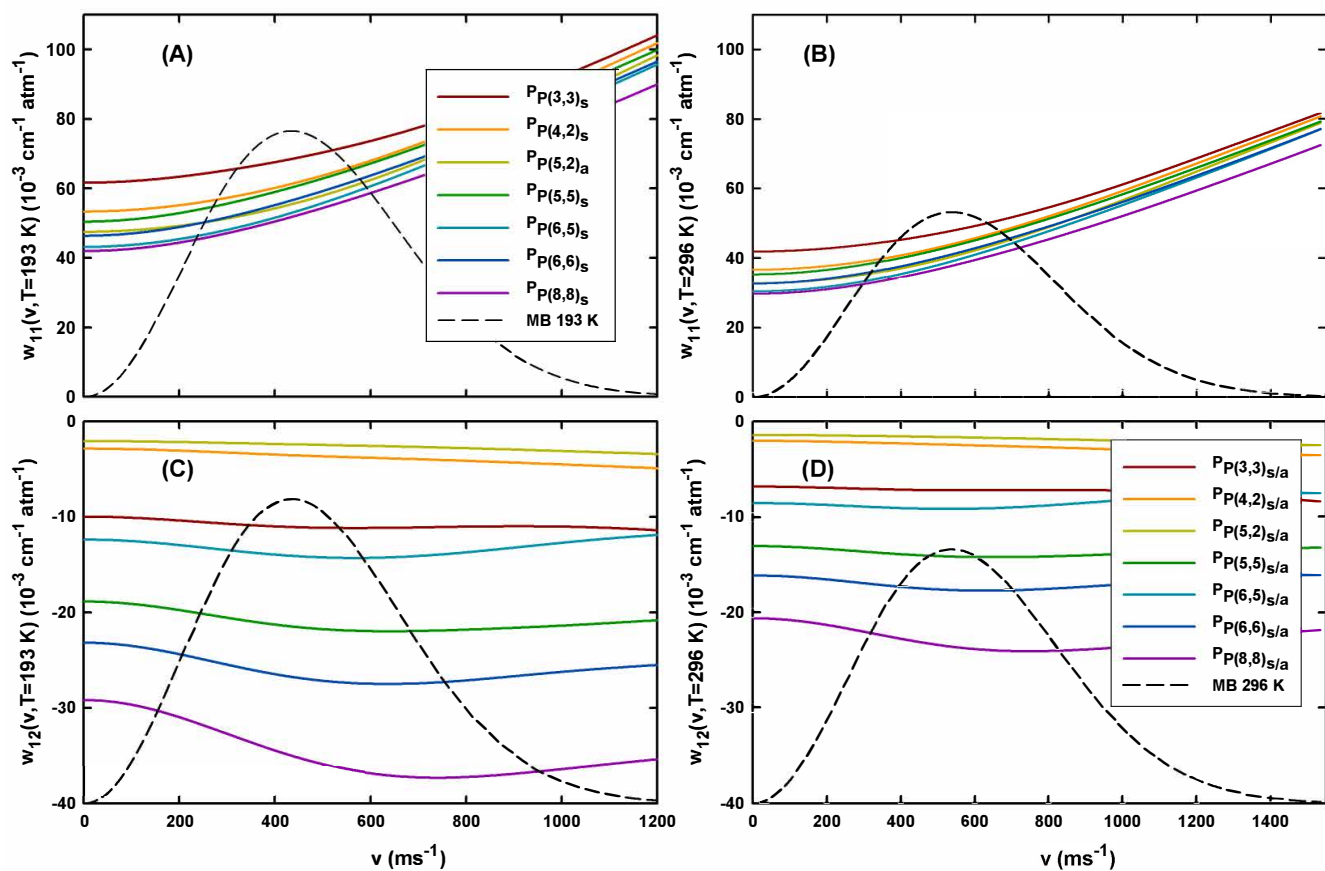


Figure 9: Speed dependence of pressure broadening parameters at 193 K and 296 K (panels A and B resp.) and of the intradoublets relaxation matrix studied at 193 and 296 K (panels C and D resp.). Results obtained with Schmuttenmaer et al. [21] PES. In each case the Maxwell - Boltzmann speed distribution is also plotted (black dashed lines).

We now discuss the speed dependence of the intradoublet relaxation matrix elements. Again as an illustrative example we consider the ${}^P P(5,5)_s$ line at 296 K. In comparison with the speed dependence of the pressure broadening coefficient of this line, the result is completely different for the intradoublet coupling as it appears from Fig. 10. Neither the quadratic nor the hypergeometric model can represent this speed dependent off diagonal relaxation matrix element $w_{12}(v, T)$ whose speed dependence is around 7% from its average value $-14 \times 10^{-3} \text{ cm}^{-1} \text{ atm}^{-1}$, see Table ???. The observed (unusual) speed dependence

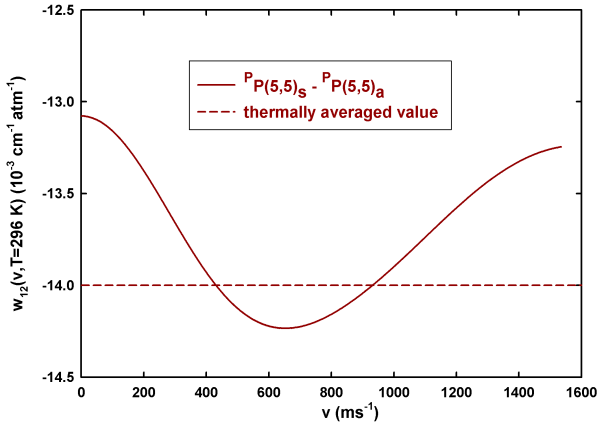


Figure 10: Speed dependence at 296 K of the relaxation matrix elements w_{12} for the ${}^P P(5,5)_{s/a}$ doublet. Results obtained with Schmuttenmaer et al. [21] PES. The thermally average value of this intradoublet line coupling coefficient is displayed with a short dashed.

can be easily explained from the fits of Fig. ???. As mentioned above two different power laws must be considered for small and high kinetic energies with two different exponents: -0.26 at small kinetic energies and -0.55 at high ones. Then using in a first step these two asymptotic behaviors we simulate according to Eqs. (??) and (17) the speed dependence of the $w_{12}(v)$ coupling term. Figure 11 shows that the fit at low kinetic energies with the exponent -0.26 clearly relates with the low (absolute) speed v while the fit at high kinetic energies providing an exponent -0.55 gives the behavior at high (absolute) speed (remind that an exponent equal to -0.5 gives no speed dependence). The combination of the 2 power laws, with a switch at 99 cm^{-1} , reproduces well the speed dependence derived from our scattering calculations. The competition between the 2 behaviors leads to a nearly cancellation of the speed dependence at 296 K.

We note that the fit of the cross sections at low kinetic energy explains the greater speed dependence observed at 193 K in Fig. 9. Results are rather similar for the other doublets as it appears from the panels C and D of Fig. 9: even if the speed dependence may vary from one doublet to the other, it remains very small, at least at room temperature. The speed dependence of the diagonal and off-diagonal relaxation matrix elements obtained with Loreau et al. PES [1] is slightly different but confirms the above conclusions.

A question remains: Is it possible to detect such a weak

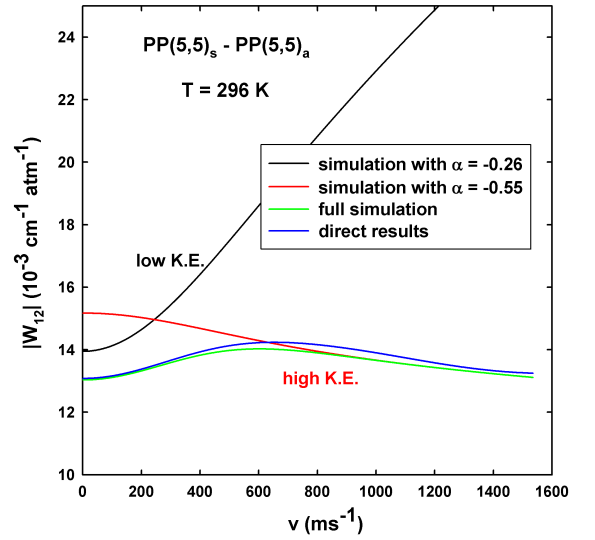


Figure 11: Comparison, at $T = 296 \text{ K}$, of the fitted speed dependent intradoublet ${}^P P(5,5)_a - {}^P P(5,5)_s$ relaxation matrix element $w_{12}(v)$ with the values derived from our CC/CS cross sections (blue line) obtained from Schmuttenmaer et al. [21] PES (absolute values, see Fig. 3 and Fig. 10).

speed dependence of the intradoublet coupling? We have therefore simulated the absorption coefficient by using the model of Ciurylo and Pine [19] and assuming uncorrelated hard collisions as done in our previous study [20]. The unperturbed line positions and the experimental intensities of the various doublets were taken from the 2016 edition of the HITRAN data base [26]. The velocity changing β rate was fixed to the corresponding value of the diagonal element $W_{11}(T)$, which is a reasonable order of magnitude (see more details in ref. [20]). Two calculations have been made: in the first one the speed dependent diagonal and coupling elements were those calculated in the present work. In the second one, the speed dependence of the coupling element was omitted and the matrix element fixed to its thermally averaged value $W_{12}(T)$.

Firstly, we consider the ${}^P P(5,5)$ doublet at 296 K. The two results are compared on the top panel of Fig. 12 for various perturber pressures. We have plotted the difference between these two absorptions relative to the peak absorption value, for two perturber pressures corresponding to an important overlapping of the two components. It is possible to compare directly with the previous works based on an identical speed dependence of the diagonal and off-diagonal elements: see figure 3 of [20]. From this comparison it appears that the amplitude of the difference between the two line shapes is reduced by a factor 10. In other words it will be impossible to detect this difference by the fitting methods developed in our previous work. From the bottom panel of Fig. 12, it seems that the ${}^P P(8,8)_{s/a}$ doublet measured at 193 K could be a more promising candidate since, on one hand the line mixing process is more important ($\frac{W_{12}}{W_{11}} = 0.63$ instead of 0.3 for the ${}^P P(5,5)_{s/a}$ doublet at 296 K). Moreover, the speed dependence of $w_{12}(v)$ is more pronounced for this doublet (see Fig. 9). The bottom panel of Fig. 12 gives the differences computed for this system. As expected,

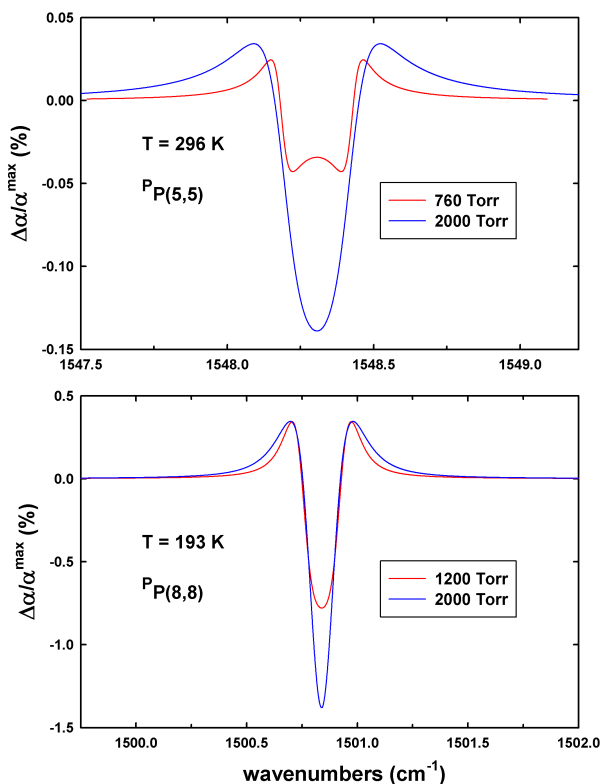


Figure 12: Differences between the absorptions computed for 0.1% of NH_3 diluted in Ar at various pressures, with and without the inclusion of the speed dependence of line mixing, relative the peak absorption value. Top: for the $^P P(5,5)_{s/a}$ doublet (alone) at 296 K. Bottom: for the $^P P(8,8)_{s/a}$ doublet (alone) at 193 K.

the amplitude of the difference is now quite comparable to that given in figure 3 of Ref. [20]. Of course, as recalled in this reference, the multispectrum fit of the data will adjust the parameters to minimize the residuals as much as possible, and the shape of residuals may be different and smaller than in Fig. 12. However, the detailed analysis provided in Ref. [20] has shown that, starting from the difference given in Fig. 12 (cf. figure 3 of [20]), it might be possible to observe a small but significant signature of the speed dependence of the coupling element (cf figures 4 and 7 of [20]). In our opinion, modern spectroscopic techniques of high sensitivity and accuracy should allow to measure such small signatures.

4. Conclusions

We have presented a first quantum *ab initio* study of some line shape parameters of a few doublets of the perpendicular ν_4 band of ammonia in argon. To this end, two potential energy surfaces have been used and lead to similar results. The obtained pressure broadening coefficients are slightly too small with respect to measured values [6, 49] but the reason is clear: our calculations suffer from the lack of rovibrational dephasing because we are not able to take into account the ν_4 vibrational mode dependence. Nonetheless, the computed thermally averaged intradoublet coupling coefficients are in overall

good agreement with the ones previously determined experimentally [6]. This type of calculations is very promising to model line mixing at low argon pressures when it is sufficient to consider such off-diagonal relaxation matrix elements. It avoids to construct the full band relaxation matrix, which would be intractable from fully *ab initio* calculations. Whereas in most of the joint experimental and theoretical accurate lineshape analyses at room temperature, the non-Voigt effects are nowadays included, the speed dependence of off-diagonal elements of the relaxation matrix are always disregarded [46, 51, 52]. In the present work, we have shown that the speed dependence of the pressure broadening coefficient is quite important and can be well represented by either the commonly used quadratic or hypergeometric models. In contrast, for the intradoublet coupling coefficients, the speed dependence is found to be small at room temperature. Therefore, we confirm the above mentioned lineshape analyses. Note that the neglect of the speed dependence of the (first order) line mixing coefficient was also theoretically justified for the pure rotational R(0) line of CO in argon [53]. It should be emphasized that conclusions cannot be drawn unless an extended range of kinetic energies, or relative speed, is considered when computed upward, downward and intradoublet cross sections. In passing, we have shown that the intradoublet cross sections can be expressed as the average of two inelastic state to state cross sections. Nevertheless, our study does not rule out the possibility of the observation of speed dependent line coupling effects on lineshapes. Such possibilities clearly depend on the system through the potential energy surface, on the collisional selection rules (more restrictive for $\text{NH}_3\text{-Ar}$ than for CO-Ar for instance), on the energy level structure and on the temperature. For instance, for the studied doublets of ammonia in argon bath the speed dependence is more pronounced at lower temperature (roughly below 193 K).

Acknowledgement

The authors thank Jean-Michel Hartmann for his continuous interest in this work. We also thank the reviewer for reminding us to mention another speed dependent parameter leading to asymmetric profiles, namely the collision time asymmetric parameter due to the finite duration of collisions. To our knowledge, the speed dependence of this parameter has only been considered in atomic line shapes, e.g. [54]. This research did not receive any specific grant from funding agencies in the public, commercial, or not-for-profit sectors.

Supplementary Material

Supplementary material associated with this article can be found, in the online version, at doi: <https://doi.org/10.1016/j.jqsrt.2022.108453>

References

- [1] J. Loreau, J. Liévin, Y. Scribano, A. van der Avoird, Potential energy surface and bound states of the $\text{NH}_3\text{-Ar}$ and $\text{ND}_3\text{-Ar}$ complexes, The Journal of Chemical Physics 141 (2014) 224303.

- [2] J. Loreau, A. van der Avoird, Scattering of NH_3 and ND_3 with rare gas atoms at low collision energy, *The Journal of Chemical Physics* 143 (2015) 184303.
- [3] Y. Belkhdja, J. Loreau, A. van der Avoird, Y. Berger, P. Asselin, Intermolecular dynamics of NH_3 -rare gas complexes in the ν_2 umbrella region of NH_3 investigated by rovibrational laser jet-cooled spectroscopy and ab initio calculations, *Phys. Chem. Chem. Phys.* 23 (2021) 10864–10874.
- [4] J.-M. Hartmann, C. Boulet, D. Robert (Eds.), *Collisional Effects on Molecular Spectra* (Second Edition), Elsevier, 2021.
- [5] J.-M. Hartmann, H. Tran, R. Armante, C. Boulet, A. Campargue, F. Forget, L. Gianfrani, I. Gordon, S. Guerlet, M. Gustafsson, J. T. Hodges, S. Kassi, D. Lisak, F. Thibault, G. C. Toon, Recent advances in collisional effects on spectra of molecular gases and their practical consequences, *Journal of Quantitative Spectroscopy and Radiative Transfer* 213 (2018) 178–227.
- [6] S. Haddad, H. Aroui, J. Orphal, J.-P. Bouanich, J.-M. Hartmann, Line broadening and mixing in NH_3 inversion doublets perturbed by NH_3 , He, Ar, and H_2 , *Journal of Molecular Spectroscopy* 210 (2001) 275–283.
- [7] S. Haddad, F. Thibault, P.-M. Flaud, H. Aroui, J. M. Hartmann, Experimental and theoretical study of line mixing in NH_3 spectra. II. Effect of the perturber in infrared parallel bands, *The Journal of Chemical Physics* 120 (2004) 217–223.
- [8] A. S. Pine, V. Markov, Self- and foreign-gas-broadened lineshapes in the ν_1 band of NH_3 , *Journal of Molecular Spectroscopy* 228 (2004) 121–142.
- [9] M. Dhib, M. Echargui, H. Aroui, J. Orphal, J.-M. Hartmann, Line shift and mixing in the ν_4 and $2\nu_2$ band of NH_3 perturbed by H_2 and Ar, *Journal of Molecular Spectroscopy* 233 (2005) 138–148.
- [10] M. Baranger, Problem of overlapping lines in the theory of pressure broadening, *Phys. Rev.* 111 (1958) 494–504.
- [11] M. Baranger, General impact theory of pressure broadening, *Phys. Rev.* 112 (1958) 855–865.
- [12] A. Ben-Reuven, Impact broadening of microwave spectra, *Phys. Rev.* 145 (1966) 7–22.
- [13] M. R. Cherkasov, Collisional interference of lines in the spectra of symmetric top molecules: I. A theory of relaxation parameters of the shape of the spectrum in the impact approximation, *Optics and Spectroscopy* 105 (2008) 851–858.
- [14] M. R. Cherkasov, Effects of collisional interference of lines in the spectra of symmetric top molecules: II. Self- and foreign-gas-broadening of rotational spectral lines, *Optics and Spectroscopy* 106 (2009) 1–9.
- [15] V. I. Starikov, Calculation of the relaxation parameters of overlapping lines of the ammonia molecule pressure broadened by argon and helium, *Optics and Spectroscopy* 114 (2013) 15–24.
- [16] Q. Ma, C. Boulet, The relaxation matrix for symmetric tops with inversion symmetry. I. Effects of line coupling on self-broadened ν_1 and pure rotational bands of NH_3 , *The Journal of Chemical Physics* 144 (2016) 224303.
- [17] Q. Ma, C. Boulet, R. Tipping, Vibrational dependence of line coupling and line mixing in self-broadened parallel bands of NH_3 , *Journal of Quantitative Spectroscopy and Radiative Transfer* 203 (2017) 425–433. HITRAN2016 Special Issue.
- [18] Q. Ma, C. Boulet, R. H. Tipping, Relaxation matrix for symmetric tops with inversion symmetry: Line coupling and line mixing effects on NH_3 lines in the ν_4 band, *The Journal of Chemical Physics* 146 (2017) 134312.
- [19] R. Ciurylo, A. S. Pine, Speed-dependent line mixing profiles, *Journal of Quantitative Spectroscopy and Radiative Transfer* 67 (2000) 375–393.
- [20] C. Boulet, J.-M. Hartmann, Toward measurements of the speed-dependence of line-mixing, *Journal of Quantitative Spectroscopy and Radiative Transfer* 262 (2021) 107510.
- [21] C. A. Schmuttenmaer, R. C. Cohen, R. J. Saykally, Spectroscopic determination of the intermolecular potential energy surface for Ar-NH_3 , *The Journal of Chemical Physics* 101 (1994) 146–173.
- [22] P. R. Berman, Speed-dependent collisional width and shift parameters in spectral profiles, *Journal of Quantitative Spectroscopy and Radiative Transfer* 12 (1972) 1331–1342.
- [23] J. Ward, J. Cooper, E. W. Smith, Correlation effects in the theory of combined Doppler and pressure broadening—I. Classical theory, *Journal of Quantitative Spectroscopy and Radiative Transfer* 14 (1974) 555–590.
- [24] H. M. Pickett, Effects of velocity averaging on the shapes of absorption lines, *The Journal of Chemical Physics* 73 (1980) 6090–6094.
- [25] F. Rohart, H. Mäder, H. Nicolaisen, Speed dependence of rotational relaxation induced by foreign gas collisions: Studies on CH_3F by millimeter wave coherent transients, *The Journal of Chemical Physics* 101 (1994) 6475–6486.
- [26] I. Gordon, L. Rothman, C. Hill, R. Kochanov, Y. Tan, P. Bernath, M. Birk, V. Boudon, A. Campargue, K. Chance, B. Drouin, J.-M. Flaud, R. Gamache, J. Hodges, D. Jacquemart, V. Perevalov, A. Perrin, K. Shine, M.-A. Smith, J. Tennyson, G. Toon, H. Tran, V. Tyuterev, A. Barbe, A. Császár, V. Devi, T. Furtenbacher, J. Harrison, J.-M. Hartmann, A. Jolly, T. Johnson, T. Karman, I. Kleiner, A. Kyuberis, J. Loos, O. Lyulin, S. Massie, S. Mikhailenko, N. Moazzen-Ahmadi, H. Müller, O. Naumenko, A. Nikitin, O. Polyansky, M. Rey, M. Rotger, S. Sharpe, K. Sung, E. Starikova, S. Tashkun, J. V. Auwera, G. Wagner, J. Wilzewski, P. Wcislo, S. Yu, E. Zak, The HITRAN2016 molecular spectroscopic database, *J. Quant. Spectrosc. Radiat. Transf* 203 (2017) 3–69.
- [27] S. Yu, J. C. Pearson, B. J. Drouin, K. Sung, O. Pirali, M. Vervloet, M.-A. Martin-Drumel, C. P. Endres, T. Shiraiishi, K. Kobayashi, F. Matsushima, Submillimeter-wave and far-infrared spectroscopy of high-J transitions of the ground and $\nu_2 = 1$ states of ammonia, *The Journal of Chemical Physics* 133 (2010) 174317.
- [28] J. M. Hutson, S. Green, Molscat version14, Collaborative Computational Project 6 of the UK Science and Engineering Research Council, Daresbury Laboratory, UK, 1995 (1995).
- [29] J. M. Hutson, C. R. Le Sueur, bound and field: Programs for calculating bound states of interacting pairs of atoms and molecules, *Comput. Phys. Commun.* 241 (2019) 1–8.
- [30] S. L. Davis, J. E. Boggs, Rate constants for rotational excitation in NH_3 -He collisions, *The Journal of Chemical Physics* 69 (1978) 2355–2366.
- [31] S. Green, Energy transfer in NH_3 -He collisions, *The Journal of Chemical Physics* 73 (1980) 2740–2750.
- [32] G. C. M. van der Sanden, P. E. S. Wormer, A. van der Avoird, J. Schleipen, J. J. ter Meulen, Close coupling calculations on rotational excitation and inversion of NH_3 by collisions with Ar, *The Journal of Chemical Physics* 97 (1992) 6460–6468.
- [33] G. C. M. van der Sanden, P. E. S. Wormer, A. van der Avoird, J. Schleipen, J. J. ter Meulen, On the propensity rules for inelastic NH_3 -rare gas collisions, *The Journal of Chemical Physics* 103 (1995) 10001–10004.
- [34] G. C. M. van der Sanden, P. E. S. Wormer, A. van der Avoird, Differential cross sections for rotational excitation of NH_3 by collisions with Ar and He: Close coupling results and comparison with experiment, *The Journal of Chemical Physics* 105 (1996) 3079–3088.
- [35] O. Tkáč, A. K. Saha, J. Loreau, D. H. Parker, A. van der Avoird, A. J. Orr-Ewing, Rotationally inelastic scattering of quantum-state-selected ND_3 with Ar, *The Journal of Physical Chemistry A* 119 (2015) 5979–5987. PMID: 25532415.
- [36] S. Green, Rotational excitation of symmetric top molecules by collisions with atoms: Close coupling, coupled states, and effective potential calculations for NH_3 -He, *The Journal of Chemical Physics* 64 (1976) 3463–3473.
- [37] S. Green, Rotational excitation of symmetric top molecules by collisions with atoms. II. Infinite order sudden approximation, *The Journal of Chemical Physics* 70 (1979) 816–829.
- [38] A. M. Richard, A. E. DePristo, Further development and application of the ECS scaling theory: Non-linear molecules, *Chemical Physics* 69 (1982) 273–293.
- [39] L. Machin, E. Roueff, Rotational excitation and de-excitation of interstellar ammonia in collisions with helium, *Journal of Physics B: Atomic, Molecular and Optical Physics* 38 (2005) 1519–1534.
- [40] A. Lévy, N. Lacome, C. Chackerian, Collisional line mixing, in: K. N. Rao, A. Weber (Eds.), *Spectroscopy of the Earth’s Atmosphere and Interstellar Medium*, Academic Press, 1992, pp. 261–337.
- [41] R. Blackmore, A modified Boltzmann kinetic equation for line shape functions, *The Journal of Chemical Physics* 87 (1987) 791–800.
- [42] R. Blackmore, S. Green, L. Monchick, Polarized D_2 Stokes-Raman Q branch broadened by He: A numerical calculation, *The Journal of Chemical Physics* 88 (1988) 4113–4119.
- [43] D. E. Manolopoulos, An improved log derivative method for inelastic scattering, *The Journal of Chemical Physics* 85 (1986) 6425–6429.
- [44] M. H. Alexander, D. E. Manolopoulos, A stable linear reference potential algorithm for solution of the quantum close-coupled equations in molecular scattering theory, *The Journal of Chemical Physics* 86 (1987)

2044–2050.

- [45] D. R. Willey, R. E. Timlin, P. G. DeNardo, P. L. Null, P. L. Pondillo, T. Tyszka, Helium pressure broadening of ammonia inversion transitions from 10 to 35 K, *The Journal of Chemical Physics* 107 (1997) 8252–8261.
- [46] A. S. Pine, Speed-dependent line mixing in the ν_3 band Q branch of methane, *Journal of Quantitative Spectroscopy and Radiative Transfer* 224 (2019) 62–77.
- [47] A. Lightman, A. Ben-Reuven, Cross relaxation in the rotational inversion doublets of ammonia in the far infrared, *Journal of Quantitative Spectroscopy and Radiative Transfer* 12 (1972) 449–454.
- [48] U. Fano, Pressure broadening as a prototype of relaxation, *Phys. Rev.* 131 (1963) 259–268.
- [49] M. Dhib, J.-P. Bouanich, H. Aroui, M. Broquier, Collisional broadening coefficients in the ν_4 band of NH_3 perturbed by He and Ar, *Journal of Molecular Spectroscopy* 202 (2000) 83–88.
- [50] S. C. M. Lujendijk, On the shape of pressure-broadened absorption lines in the microwave region. i. deviations from the lorentzian line shape, *Journal of Physics B: Atomic and Molecular Physics* 10 (1977) 1735–1739.
- [51] J. W. Brault, L. R. Brown, C. Chackerian, R. Freedman, A. Predoi-Cross, A. S. Pine, Self-broadened $^{12}\text{C}^{16}\text{O}$ line shapes in the $\nu=2\leftarrow 0$ band, *Journal of Molecular Spectroscopy* 222 (2003) 220–239.
- [52] J. Domysławska, S. Wójtewicz, K. Bielska, S. Bilicki, R. Ciuryło, D. Lisak, Line mixing in the oxygen B band head, *The Journal of Chemical Physics* 156 (2022) 084301.
- [53] E. A. Serov, N. Stolarczyk, D. S. Makarov, I. N. Vilkov, G. Y. Golubiatnikov, A. A. Balashov, M. A. Koshelev, P. Wcisło, F. Thibault, M. Y. Tretyakov, CO-Ar collisions: ab initio model matches experimental spectra at a sub percent level over a wide pressure range, *Journal of Quantitative Spectroscopy and Radiative Transfer* 272 (2021) 107807.
- [54] A. Bielski, R. Ciuryło, J. Domysławska, D. Lisak, R. S. Trawiński, J. Szudy, Laser-induced fluorescence study of collision-time asymmetry and speed-dependent effects on the ^{114}Cd 326.1-nm line perturbed by Xe, *Phys. Rev. A* 62 (2000) 032511.